Int. J. Electrochem. Sci., 17 **(2022)** Article Number: 221038, doi: 10.20964/2022.10.07

International Journal of
ELECTROCHEMICAL
SCIENCE
www.electrochemsci.org

Influence of Microstructure on Corrosion Behavior of Zn-Al-Sr Alloys in Sodium Chloride Solution

J. Gutiérrez-Menchaca[1], *J. A. Cabral-Miramontes*[2,*], *A. M. Garay-Tapia*[1], *D. Torres-Torres*[1], *C. GaonaTiburcio*[2], *J.M. Jaquez-Muñoz*[2], *F. Almeraya-Calderón*[2,*]

[1] Centro de Investigación en Materiales Avanzados S.C. (CIMAV), Unidad Monterrey, Alianza Norte 202, Parque PIIT, Apodaca, Nuevo León., C.P., 66629, México.
[2] Universidad Autónoma de Nuevo León, Facultad de Ingeniería Mecánica y Eléctrica, Centro de Investigación e Innovación en Ingeniería Aeronáutica (CIIIA), Av. Universidad s/n, Ciudad Universitaria, San Nicolás de los Garza, Nuevo León 66455, México
[*]E-mail: facundo.almerayacld@uanl.edu.mx /jose.cabralmr@uanl.edu.mx

Received: 1 July 2022 / *Accepted:* 4 August 2022 / *Published:* 10 September 2022

The present research objective is to evaluate microstructure's influence on corrosion behavior of a new series of Zn-Al-Sr alloys with possible coating applications. Conventional casting procedures prepared four Zn-Al-Sr alloys. The alloys were Zn-1Al-0.05Sr, Zn-2.5-Al-0.1Sr, Zn-4.5-Al-0.5Sr, and Zn 10Al 1Sr. Microstructural characterization was performed by scanning electron microscopy. Corrosion behavior was evaluated employing electrochemical techniques such as potentiodynamic polarization (PP) and electrochemical impedance spectroscopy (EIS). The alloys were exposed to 3.5 wt. % NaCl. Results indicated that all samples presented the η-Zn, α-Al, and SrZn13 phases in different arrangements depending on the alloy composition. Electrochemical tests revealed that Al increased alloy corrosion resistance by forming insoluble oxides, whereas Sr improved corrosion product layer compactness and homogeneity of the corrosion product layer. However, the large grain size of the SrZn13 compound favored the corrosion process by galvanic coupling. Compositions between 2.5 and 4.5 wt.% Al and 0.05 and 0.5 wt.% Sr exhibited the highest corrosion resistance of the Zn-Al-Sr alloys in 3.5 wt.% NaCl solution, lower Sr content promoted both homogenous corrosion and a compacted corrosion products layer. A high density of intermetallic particles adversely affects Zn-Al-Sr alloys corrosion resistance, and Sr content must not exceed 0.5 wt.%.

Keywords: Zn-Al-Sr alloys, SrZn13 compound, corrosion resistance, Potentiondynamic Polarization, EIS

1. INTRODUCTION

Zn-Al base alloys are widely used as protective coatings on steels for structural and automotive applications. These coatings have shown superior corrosion performance than to their equivalent Al-Si

coatings since Zn acts as a sacrificial material [1,2]. The formation of insoluble Zn and Al oxides also delays environmental corrosion and increases the lifetime of steel substrates. An important body of research has investigated the corrosion behavior of Zn Al coatings [3,4]. In particular, Galfan (Zn-5wt.% Al) and Galvalume (55Al-43.5 wt.% Zn-1.5 wt.% Si) coatings can work as a protective barrier as well as a sacrificial material for steel [5,6].

Additionally, adding elements as an alloying is one of the most practical ways to enhance alloys' protective properties. Elements such as Mg, Ti, Ni, and rare earth can affect the electrochemical response, tribological properties, and thermal stability, among others [1,7,8,9]. For instance, additions of Mg (1 – 3 wt.%) have demonstrated extra corrosion resistance forming a stable oxide layer [10]. This layer is generated due to the dissolution of Mg-containing phases dissolution, such as Mg_2Zn_{11} and $MgZn_2$, where free Mg ions react with the oxidizing environment [11].

Recently, Sr has captured a great deal of attention because of its ability to modify both mechanical and electrochemical properties of Zn-based alloys at relatively low amounts (0.05 - 1.5 wt.% Sr) [12,13,14]. According to Liu-et al. 2018, small amounts of Sr (0.1-0.15 wt.% Sr) can promote a more uniform corrosion process and reduce the stress concentration of Zn-4Al alloy, resulting in better mechanical integrity. The uniform and compact protective layer formed on Zn-Al-Sr alloys prevents localized corrosion and discloses better corrosion behavior than cast Zn-Mg alloys [15]. The evaluation of the electrochemical response of Zn-Al-Sr alloys has only been studied on simulated body fluids (Hank's solution), and no reports regarding other solutions have been found. Often, steel components are exposed to deicing salts, marine atmospheres, and different environments containing chlorides. Therefore, assessing the electrochemical behavior of Zn-Al-Sr alloys in saline solutions is crucial.

Given that Sr is commonly added in master alloy form at the industrial level, various proportions of Al-10Sr master alloy were added to zinc to study the electrochemical behavior of Zn-Al-Sr alloys.

This work aimed to evaluate the microstructure's influence on corrosion behavior of Zn-1Al-0.05Sr, Zn-2.5-Al-0.1Sr, Zn-4.5-Al-0.5Sr, and Zn 10Al 1Sr alloys. SEM was used to characterize the microstructure, and electrochemical methods such as potentiodynamic polarization (PP) and electrochemical impedance spectroscopy (EIS) were used to study corrosion behavior. The alloys were subjected to a solution of 3.5 weight percent NaCl.

2. MATERIALS AND METHODS

2.1 Materials

Ternary Zn-Al-Sr alloys were prepared by melting down high purity ingots of Zn (99.98 %), Al (99.9 %), and Al-10Sr master alloy for one hour at 600 °C in an electrical furnace called the VBF-1200X. After being mechanically agitated, the molten alloy was poured into a steel mold made of unheated steel. Inductively coupled plasma atomic emission spectroscopy (ICP-AES) in a thermal Electron-ICAP spectrometer was used to determine the nomenclature and chemical composition of the produced alloys, as shown in Table I.

Table 1. Chemical composition of the as-cast Zn-Al-Sr alloys (wt.%)

Alloys	Al	Sr	Zn
Zn-1Al-0.05Sr	1.11 ±0.0015	0.03 ±0.0555	Balance
Zn-2.5Al-0.1Sr	2.43 ±0.0075	0.15 ±0.1215	Balance
Zn-4.5Al-0.5Sr	4.52 ±0.0334	0.67 ±0.2260	Balance
Zn-10Al-1Sr	9.10 ±0.0490	0.98 ±0.4550	Balance

2.2 Microstructural Characterization

Specimens were manufactured following ASTM E3-11[16] and cut from a bulk ingot. Various SiC grit papers were used for polishing (180, 400, 600, and 800). The Kroll solution, which contains HF 3 mL, HNO3 5 mL, and water 100 mL, was used to etch the polish sample. SEM images produced with a backscattered electron (BSE) detector were used for the microstructural study, which was done using Scanning Electron Microscopy (SEM, Jeol JSM-6010PLUS/LA) operating at 20 kV with a 1000x magnification, WD = 14 mm.

2.3 Electrochemical Test

Electrochemical tests were carried out at room temperature using Solartron 1286 equipment and a 1260 phase gain analyzer. Casting samples served as the working electrodes in a traditional three-electrode cell design. The reference and counter electrodes were a saturated calomel electrode (SCE) and a platinum mesh. The test solution contained 3.5-weight percent NaCl. At a sweep rate of 0.06 V min-1 and a potential scan range of between -0.8 and +1.8 V versus, potentiodynamic polarization curves (PPC) were captured, ASTM G5-13 was followed for applying SCE [17,18,19,20]. The frequency range of the EIS measurements was 10 mHz to 100 kHz, with 10 points per decade and a perturbation amplitude of 10 mV [21,22,23]. Using the "Zview" program, the EIS spectrums were examined in terms of an equivalent circuit three copies of each corrosion test were run.

3. RESULTS AND DISCUSSION

3.1 SEM microstructural analysis

The microstructure of the as-cast Zn-Al-Sr alloys is shown in Figure 1. All alloys consisted of a primary proeutectic phase surrounded by a lamellar eutectic structure (α-Al + η-Zn). The η-Zn phase corresponded to the primary proeutectic of Zn-1Al-0.05Sr, Zn-2.5Al-0.1Sr, and Zn 4.5Al 0.5Sr alloys, whereas α'-Al phase corresponded to the primary proeutectic of Zn-10Al-1Sr alloy. The Zn-1Al-0.05Sr alloy (Figure. 1a) shows coarse dendrites of the η-Zn phase surrounded by a low proportion of eutectic structure. For the Zn-2.5Al-0.1Sr alloy (Figure 1(b)), the size of the dendrites was reduced by increasing

the Al and Sr content, whereas the fraction of the eutectic structure was increased. A sharp-edged phase was found in the intergranular regions, which was attributed to a $SrZn_{13}$ intermetallic compound [14]. Subsequently, a continuous reduction of the primary phase was observed in the Zn-4.5Al-0.5Sr alloy (Figure 1c), while the proportion of eutectic structure and $SrZn_{13}$ intermetallic compound increased.

The Zn-10Al-1Sr alloy exhibited a microstructure composed of α'-Al dendrites and secondary phases in the interdendritic regions (Figure 1(d)). Nevertheless, the α'-Al phase is not stable at room temperature because the excess zinc in its crystalline structure (up to 67 wt.% Zn) decomposing into the α´-Al and ηZn phases through the monotectoid reaction (~277 °C) [24]. Thus, a different arrangement of phases was observed in the Zn-10Al-1Sr alloy.

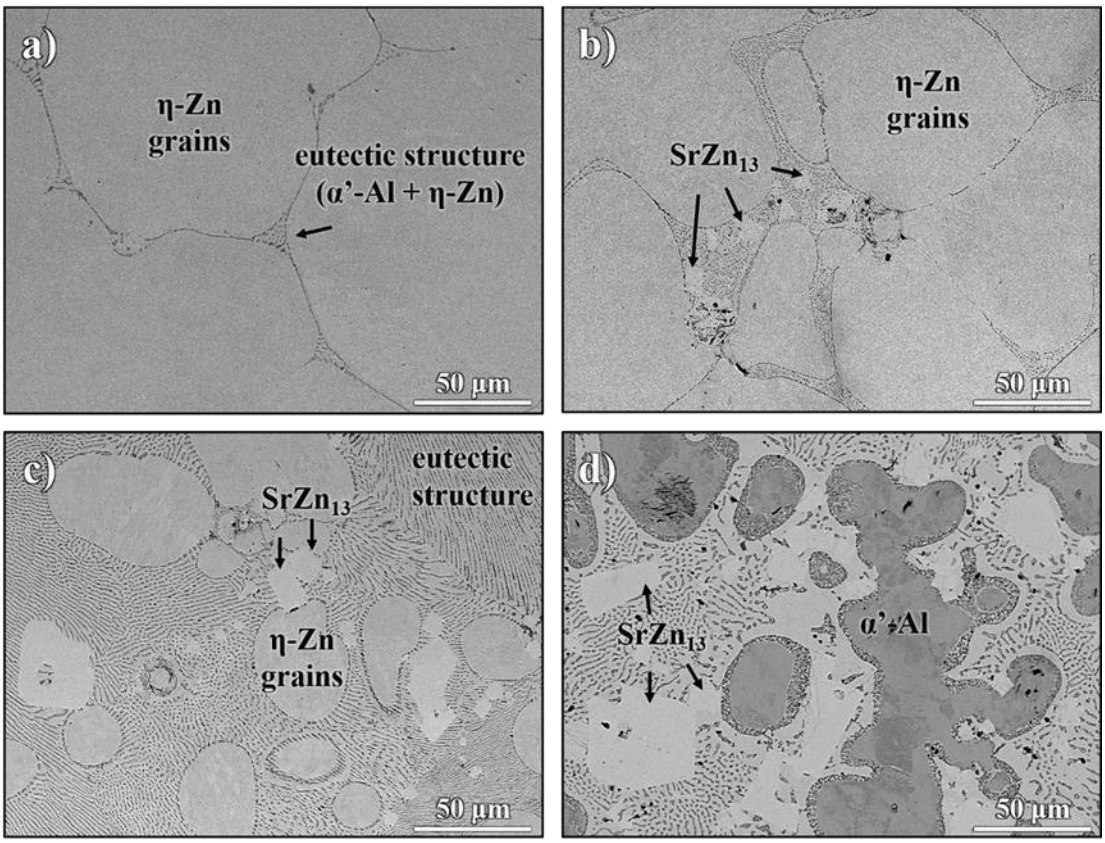

Figure 1. SEM-BSE microstructure of the alloys at a magnification of 1000x: (a) Zn-1Al-0.05Sr; (b) Zn-2.5Al-0.1Sr; (c) Zn-4.5Al-0.5Sr; and (d) Zn-10Al-1Sr.

The image analysis obtained the average grain size of the proeutectic phase, and the proportion of the eutectic structure was obtained by image analysis see Figure 2. The grain size of the proeutectic phase decreased with increasing the Al and Sr content, whereas the lamellar eutectic structure initially increases but decreases above 4.5 wt.% Al and 0.5 wt.% Sr. When increasing the Sr content, the SrZn13 intermetallic phase showed a mean particle size range between 10.6 ± 3.7 and 18.1 ± 2.7 µm [see Figure 1(b) and 1(d)].

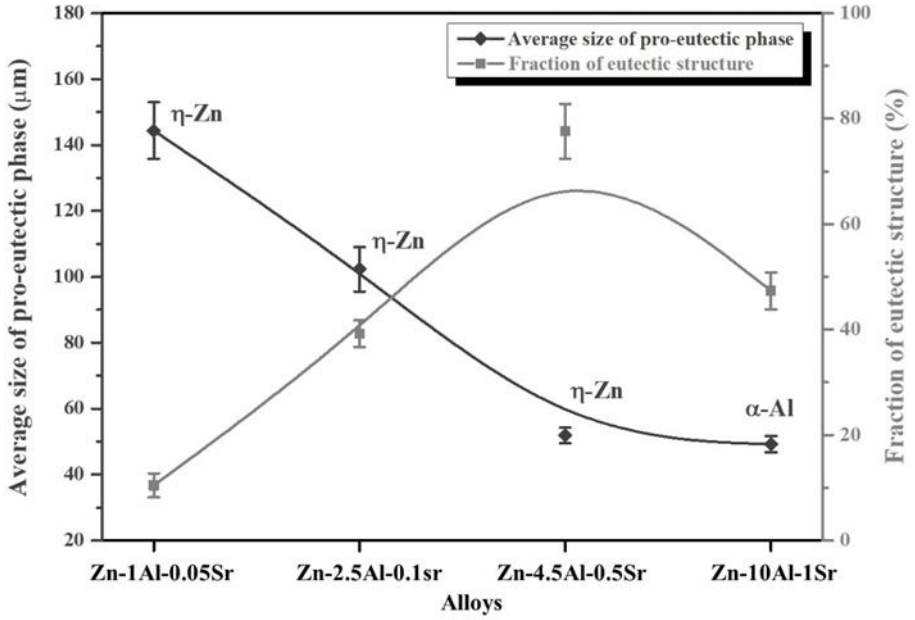

Figure 2. Average size of proeutectic phase and fraction of the eutectic structure at different Zn-Al-Sr composition.

3.2 Electrochemical measurements

3.2.1 Potentiodynamic Polarization

In PP curves, the analysis gives information about the corrosion rate and mechanism. The Tafel extrapolation was used in potentiodynamic polarization to determine the i_{corr} ($A \cdot cm^{-2}$), and corrosion rate [25-28].

The studied Zn-Al-Sr alloys potentiodynamic polarization curves (PPC) in 3.5 %wt. NaCl solution are shown in Figure 3. Corrosion potential (E_{corr}), corrosion current density (i_{corr}), and passivation current density (i_{pass}) were obtained from the Tafel extrapolation method [19,25,26], and these parameters are given in Table 2. PPC plots revealed that the (a) Zn-1Al-0.05Sr, (b) Zn-2.5Al-0.1Sr, and (c) Zn-4.5Al-0.5Sr alloys showed E_{corr} values between -1.27 and -1.28 V (curves (a), (b), and (c) in Figure 3, respectively). In contrast, the (d) Zn-10Al-1Sr alloy presented a more negative E_{corr}, -1.43 V (curve (d) in Figure 3). Corrosion potential is directly correlated with corrosion process susceptibility, where the more positive corrosion potential, the less susceptibility to corrosion [29]. The corrosion susceptibility Zn-Al-Sr alloys was as follows: (a) Zn-1Al-0.05Sr = (b) Zn-2.5Al-0.1Sr < (c) Zn-4.5Al0.5Sr < (d) Zn-10Al-1Sr, where the (d) Zn-10Al-1Sr alloy displayed the highest corrosion susceptibility. The (a) Zn-1Al-0.05Sr and (b) Zn-2.5Al-0.1Sr alloys showed higher amounts of primary η-Zn phase, which acts as a sacrificial anode once the α-Al phase is passivated. Afterward, the corrosion susceptibility increases due to the increase of secondary phases by further addition of Al and Sr.

Likewise, i_{corr} decreases from 2.23×10^{-5} to 1.74×10^{-5} $A \cdot cm^{-2}$ when the Al and Sr content increases from 1 wt.% Al and 0.05 wt.% Sr to 2.5 wt.% Al and 0.1 wt.% Sr. Nevertheless, i_{corr} increased to 63.87×10^{-5} $A \cdot cm^{-2}$ at the highest addition of Al and Sr (10 wt.% Al and 1.5 wt.% Sr). Since i_{corr} and

the corrosion rate have a proportional relation, the (b) Zn-2.5Al-0.1Sr alloy present the best performance in corrosion resistance of all Zn-Al-Sr alloys, whereas the (d) Zn-10Al-1Sr alloy was the worst.

All samples exhibited a passivation process at the anodic region (see Figure 3), mainly caused by the formation of the corrosion products layer at the sample/solution interface. The layer can provide extra corrosion protection; its protection level will depend on its thickness, density, and porosity. The (a) Zn-1Al-0.05Sr alloy showed a passivation region between -1.24 and -1.13 V. The i_{pass} was maintained close to 1.31×10^{-5} A·cm^{-2} (curve (a) in Figure 3). Above pitting potentials, passivity breakdown occurs, allowing the charge transfer to increase with increasing potential. The (b) Zn-2.5Al-0.1Sr alloy showed three stages of passivation: main passivation, breakdown, and re-passivation (curve (b) in Figure 3). During passivation, current density decreased continuously up to 0.75×10^{-5} A·cm^{-2}, indicating the continuous formation of corrosion products. The double passivation effect is probably caused by forming new corrosion products, which fill-pores of the degraded corrosion product layer [30]. The curve of the (c) Zn-4.5Al-0.5Sr alloy also presented a passivation region but no re-passivation process. Finally, the (d) Zn-10Al-1Sr alloy showed a passivation region between -1.30 and -1.05 V and an i_{pass} of 56.07×10^{-5} A·cm^{-2} (curve (d) in Figure 3). This alloy presented the widest passivation region regarding the potential of Zn-Al-Sr alloys, but i_{pass} was considerably larger, indicating increased charge transfer.

The increase in the corrosion current density (i_{corr}) of the Zn-10Al-1Sr alloy may be due to two main factors. The first is related to the lamellar eutectic phase fraction (β+η) that plays an important role in the corrosion resistance of Zn-Al alloys. When the dissolution of the η-Zn phase begins, the Zn-based oxide layers formed are porous and are not well adhered to the surface, therefore, they do not protect the material against aggressive environments [31-32]. In this case, the corrosive medium can diffuse continuously through the porous layer and react with the substrate, increasing the galvanic correction inside. With this process, the corrosion products block the pores of the formed layer and generate autocatalytic corrosion cells, which result in severe localized corrosion processes and therefore increase the i_{corr} [33]. Second, when forming the SrZn13 phase, it does so discontinuously and has a lower electrical potential than the η-Zn phase. Which causes the $SrZn_{13}$ phase to dissolve as a sacrificial anode. Therefore, in the Zn-10Al-1Sr detection, there is a greater amount of SrZn13 phase located in a discontinuous manner that acts as a sacrificial anode and this can cause the highest i_{corr} in this alloy.

Based on this, the higher corrosion current density presented by the Zn-10Al-1Sr sample could be due to a decrease in the fraction of the lamellar eutectic phase (β+η) and an increase in the grain size of the primary phase η-Zn. The presence of 1% by weight of Sr has a detrimental effect on the corrosion resistance of the Zn-Al-Sr alloy. Thus, the corrosion products layer on the (a) Zn-1Al-0.05Sr, (b) Zn-2.5Al-0.1Sr, and (c) Zn-4.5Al-0.5Sr alloys was more homogeneous and compact than that formed on the (d) Zn-10Al-1Sr alloy.

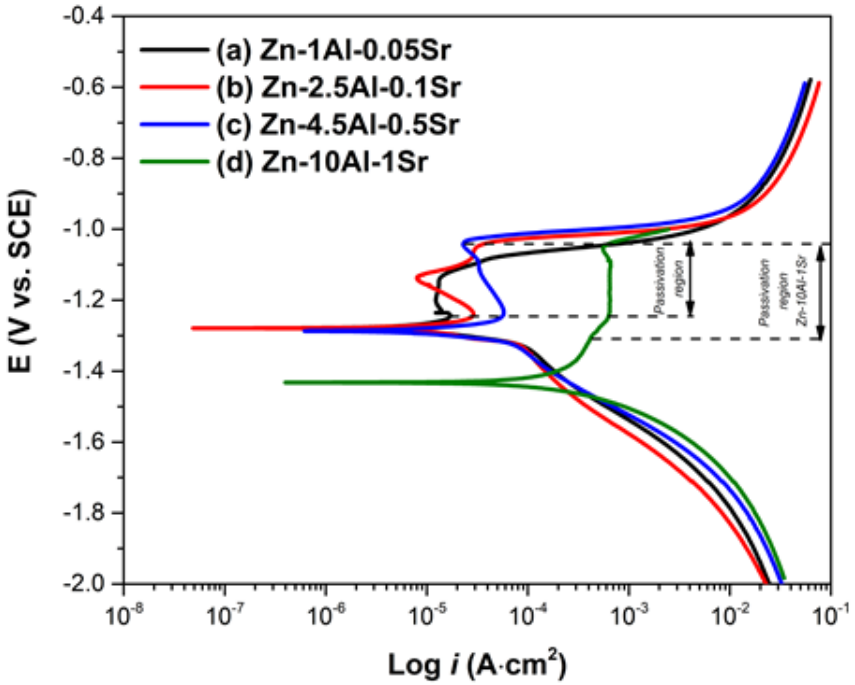

Figure 3. Potentiodynamic polarization curves (PPC) for Zn-1Al-0.05Sr, Zn-2.5-Al-0.1Sr, Zn-4.5-Al-0.5Sr, and Zn 10Al 1Sr alloys immersed in 3.5 wt.% NaCl solution.

Table 2. Electrochemical parameters obtained by PCC analysis immersed in 3.5 wt.% NaCl.

Alloy	E_{corr} (V)	i_{corr} (A·cm^{-2})	i_{pass} (A·cm^{-2})
Zn-1Al-0.05Sr	-1.273	2.23×10^{-5}	1.31×10^{-5}
Zn-2.5Al-0.1Sr	-1.275	1.74×10^{-5}	0.755×10^{-5}
Zn-4.5Al-0.5Sr	-1.289	4.16×10^{-5}	2.27×10^{-5}
Zn-10Al-1Sr	-1.431	63.87×10^{-5}	63.93×10^{-5}

3.3 Electrochemical Impedance Spectroscopy

Figure 4 shows the Nyquist and Bode plots recorded for the Zn-Al-Sr alloys. All plots show one capacitive loop at high frequencies and a non-well-defined capacitive loop at low frequencies [Figures 4(a) and 4(b)].

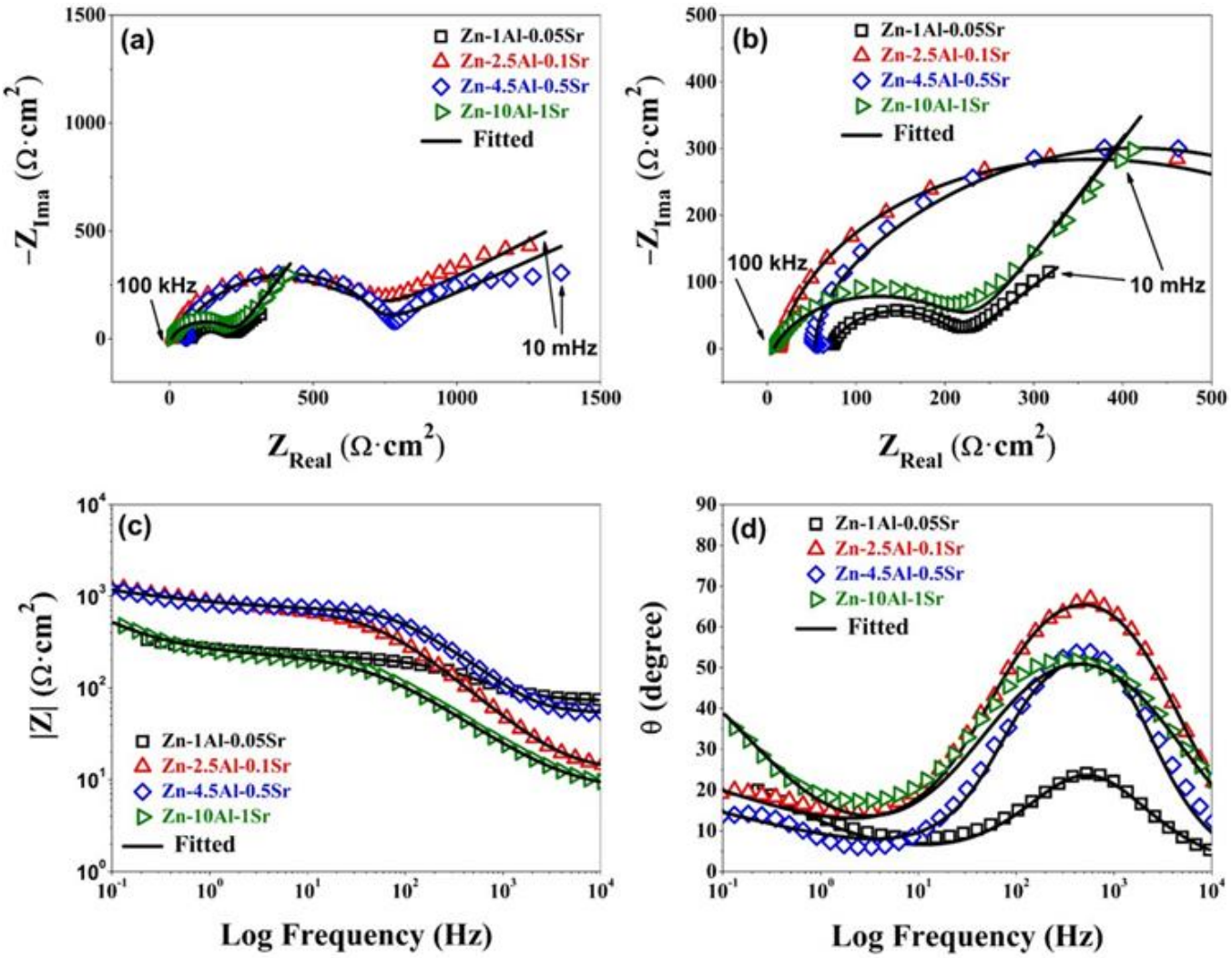

Figure 4. Measured data and fitted values of electrochemical impedance spectroscopy for Zn-1Al-0.05Sr, Zn-2.5-Al-0.1Sr, Zn-4.5-Al-0.5Sr, and Zn 10Al 1Sr alloys. (a) Nyquist plots; (b) magnification of Nyquist plots; (c) Bode plot (impedance vs. frequency); and (d) Bode plot (phase angle vs. frequency);

Bode plots of |Z| vs. frequency (Figure 4(c)) and angle phase vs. frequency (Figure 4(d)) suggested one time constant at high frequencies and a non-well-defined time constant at low frequencies in all spectra. The time constant at high frequencies was correlated to the charge transfer process, which is controlled by the ionic double layer capacitance [34-35]. Likewise, the time constant at low frequencies was associated with diffusional processes [36-37]. The diameter of the capacitive loop at high frequencies increases with the Al and Sr content but decreases above 4.5 wt.% Al and 0.5 wt.% Sr (Figures 4(a) and 4(b)). Since the capacitive diameter is directly correlated with corrosion resistance, i.e., the larger the diameter, the higher the resistance to corrosion, the corrosion resistance of alloys increased with augmenting Al and Sr but is seriously affected with excessive amounts of Al and Sr.

Fitting EIS spectra data proposed an equivalent electrical circuit (EEC) to obtain the impedance parameters, see Figure 5. R_s is the solution resistance; R_{ct} and CPE (constant phase element) are the resistance and capacitance of the time constant at high frequencies, and W1 corresponds to the Warburg impedance. The impedance of CPE can be estimated as follows [38-39]:

$$(\omega) = [(j\omega)]^{-1} \quad (1)$$

Where the magnitude of CPE is Y, the square root of -1 is j, ω = 2πf is the angular frequency (f in Hz), and n corresponds to the depression degree of impedance spectra. When n = 1, CPE behaves as pure capacitor; n = 0, as pure resistor; and n = 0.5, as Warburg impedance [40-42].

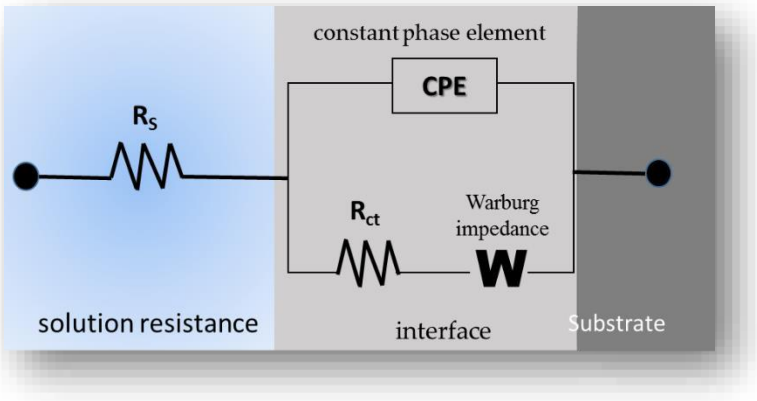

Figure 5. Equivalent electrical circuit (*EEC*).

The fitted EIS parameters are given in Table 3. The proposed EEC successfully characterized EIS data since the error was less than 5 %, and the standard deviation (χ^2) was in the order of 10^{-3} [4] Additions up to 4.5 wt.% Al and 0.5 wt.% Sr increased the corrosion resistance of Zn-Al-Sr alloys, but further additions decreased its corrosion resistance. Quantitative analysis using Bode diagrams (Figures 4(c) and 4(d)) confirms the above.

Table 3. Fitted parameters were obtained from the EEC for all EIS data.

Alloys	R_s, **Ω·cm²**	*CPE*, **μF·cm⁻²**	*n*, **0 < *n* < 1**	R_{ct}, **Ω·cm²**	W_1, **kΩ·cm²**	*Error*, **%**	χ^2
Zn-1Al-0.05Sr	71.80	12.52	0.84	139.5	0.76	3.33	0.94
Zn-2.5Al-0.1Sr	12.52	8.36	0.89	599.5	3.94	1.14	1.08
Zn-4.5Al-0.5Sr	47.22	4.85	0.88	708.3	1.76	1.28	0.71
Zn-10Al-1Sr	7.64	59.8	0.76	225.3	1.60	2.12	8.62

Additionally, Zn-2.5Al-0.1Sr and Zn-4.5Al-0.5Sr alloys showed low CPE values, indicating a more homogeneous corrosion product layer. On the other hand, the Zn-10Al-1Sr alloy displayed a higher CPE value, indicating the presence of defects (e.g., cracks and pores) on the corrosion products layer. Large R_{ct} and low CPE values are associated with a compact and homogeneous corrosion product layer

[43]. This is consistent with the observations in potentiodynamic polarization curves. Also, Nyquist spectra seem to present an oblique line close to 45° at lower frequencies, which resembles the form of Warburg impedance (W1) see Figure 4(b). The Warburg impedance indicates defects on the corrosion products layer, affecting its compactness. Additionally, W1 was measured at lower frequencies, revealing that diffusion processes control corrosion.

As the Al content increased, the proportion of α-Al phase in the Zn-Al-Sr alloys increased. As a result, the corrosion resistance of these alloys was improved. This behavior is mainly attributed to the formation of insoluble oxides on the surface of the alloys, which offers additional protection against corrosion. Likewise, the corrosion products layer presented better corrosion resistance at lower Sr content [44,45]. Nevertheless, at the highest Sr content, a high density of $SrZn_{13}$ grains was observed, and the corrosion process is favored possibly by galvanic coupling. According to the standard electrode potential (vs. standard hydrogen reference), Zn, Al, and Sr present potentials of -0.762, -1.70, and 2.92 V, respectively [46,47]. Therefore, the Sr-containing phase ($SrZn_{13}$) corrodes preferentially before η-Zn and α-Al phases, thus acting as a sacrificial anode. Subsequently, the α-Al phase is passivated, and the η-Zn phase is corroded. However, the corrosion resistance of the Zn-10Al-1Sr alloy was seriously affected mainly by pitting corrosion, which is promoted by the large grain size and non-uniform distribution of the $SrZn_{13}$ grains. Thus, rapid degradation of the corrosion products layer is observed (curve (d) in Figure 3). During pitting corrosion. Cl^- anions contaminate the corrosion products layer, making the corrosion process auto-catalytic [48-50]. All samples presented a corrosion products layer undermined by vacancies formation and rapid cation release at the film/solution interface. This result was confirmed by EIS measurements, where all the spectra showed a flattening at low frequencies (Figure 4).

4. CONCLUSIONS

In this research, the effect of microstructure on the corrosion behavior of Zn-Al-Sr alloys has been investigated by electrochemical measurements in the alloy model.

- All alloys presented the η Zn, α-Al, and $SrZn_{13}$ phases but were arranged differently according to the composition of the alloys.
- The results indicated that the PPC and EIS measurements showed that the electrochemical response of Zn-Al-Sr alloys was susceptible to microstructure, particularly with the grain size and distribution of the $SrZn_{13}$ compound.
- Addition Al increased the corrosion resistance of Zn-Al-Sr alloys by forming insoluble oxides. At the same time, Sr promoted a more homogeneous and compact corrosion product layer.
- Large grains of $SrZn_{13}$ promoted corrosion by galvanic coupling, which may be responsible for the poor performance of Zn-10Al-1Sr alloy.
- It is necessary to consider options for Al adding due to the toxicity of this element in the human body reported by different authors (it can produce Alzheimer's).

ACKNOWLEDGMENTS
The authors would like to thank the Mexican National Council for Science and Technology (CONACYT) for the support provided for developing the projects A1-S-8882, the UANL-CA-316 working group, and Universidad Autónoma de Nuevo León (UANL) for the facilities given to developing this investigation.

References

1. C. Yao, H. Lv, T. Zhu, W. Zheng, C. Yuan and W. Gao. *J. Alloys Compd.*, 670 (2016) 239.
2. Y. Xie, A. Du, X. Zhao, R. Ma, Y. Fan and X. Cao. *Surf. Coat. Technol.*, 337 (2018) 313.
3. S. Shibli, B. Meena and R. Remya. *Surf. Coat. Techno.l*, 262 (2015) 210.
4. Z. Cao, G. Kong, C. Che and Y. Wang. *Appl. Surf. Sci.*, 426 (2017) 67.
5. C.W. Lee and B.C. De Cooman. *Metall Mater Trans A*, 45(2004) 4499.
6. J.K. Chang, C.S. Lin and W.R. Wang. *Surf. Coat. Technol.*, 350 (2018) 880.
7. H.M. Abd El-Lateef, A.R. El-Sayed and H.S. Mohran. *Nonferr Metal Soc.*, 25 (2015) 8, 2807.
8. Y. Han, Y. Xia, X. Chen, L. Sun, D. Liu, X. Ge, X. *Anti-Corros Method M*, 65 (2018) 2, 131-137.
9. M. Zhang, G. Zhou, H. Sun, X. Teng and Z. Zhao. *Materials*, 7 (2020) 026525.
10. T. Prosek, J. Hagström, D. Persson, N. Fuertes, F. Lindberg, O. Chocholatý, C. Taxén, J. Šerák and F. Thierry. *Corros Sci.*, 110 (2016) 71.
11. K. Nowacki, H. Kania, K. Wieczorek and A. Smalcerz, A. *Solid State Phenom, Trans Tech Publ.*, 246 (2016) 143.
12. Y. Liu, C. Geng, Y. Zhu and X. Chen. *J. Alloys Compd.*, 695 (2017) 443.
13. Y. Liu, Z. Yin, Y. Liu, C. Geng, X. Chen, J. Xu and J. Peng. *Int. J. Electrochem. Sci.*, 13 (2018) 1640.
14. J. Gutiérrez-Menchaca, D. Torres-Torres and A. Garay-Tapia. *J. Alloys Compd.*, 829 (2020) 154511.
15. X. Liu, J. Sun, K. Qiu, Y. Yang, Z. Pu, L. Li and Y. Zheng. *J. Alloys Compd.*, 664 (2016) 444.
16. ASTM E3-01. (2009), "Standard guide for preparation of metallographic specimens", *ASTM International: West Conshohocken, PA, USA*,
17. ASTM G5-11. (2011), "Standard reference test method for making potentiostatic and potentiodynamic anodic polarization measurements", *ASTM International: West Conshohocken, PA, USA*,
18. J. Cabral-Miramontes, F. Almeraya-Calderón, F.E. López, M. Lara Banda, J. Olguín-Coca, L.D. López-León, I. Castañeda-Robles, M.A.E Alcalá, P. Zambrano-Robledo, C. Gaona-Tiburcio. *Metals*, 11 (2021) 1838.
19. ASTM G102-89. (1999), "Standard practice for calculation of corrosion rates and related information from electrochemical measurements", ASTM International: West Conshohocken, PA, USA.
20. M. Lara-Banda, C. Gaona-Tiburcio, P. Zambrano-Robledo, M. Delgado-E 1, J. A. Cabral-M, D. Nieves-M, E. Maldonado-B, F. Estupiñan-L, J. G. Chacón-Nava, F. Almeraya-Calderón. *Materials*, 13 (2020) 2836.
21. ASTM G106-15. (2015), "Standard practice for verification of algorithm and equipment for electrochemical impedance measurements", ASTM International: West Conshohocken, PA, USA.
22. C. Gaona-Tiburcio, M. Montoya R., J.A. Cabral M., F. Estupiñan L., P. Zambrano R., R. Orozco C., J.G. Chacon-Nava, M.A. Baltazar Z., F. Almeraya-Calderon *Coatings*, 10 (2020) 521.
23. F. Almeraya-Calderón., M. Montoya-R, N. Garza Montes de Oca1., J.H. Castorena G., F. Estupiñan L., J.Cabral M., E. Maldonado B and C. Gaona-Tiburcio. *Int. J. Electrochem. Sci.*, (2019) 9596 – 9609.
24. Y. H. Zhu. *Mater Trans.*, 45 (2004) 3083-3097.

25. A. Cabral Miramontes, C. A. Poblano Salas, G. K. Pedraza Basulto, C. Gaona Tiburcio, P. Zambrano Robledo and F. Almeraya Calderón. *Aircraft Aircr*., 90 (2018) 2, 336-343.
26. C. Wagner and W. Traud, Zeitschrift Für Elektrochemie Und Angew. Phys. Chemie., 44 (1938) 391.
27. J. A. V. Butler, Trans. Faraday Soc., 19 (1924) 729.
28. J. M. Jáquez-Muñoz, C. Gaona-Tiburcio, J. Cabral-Miramontes, D. Nieves-Mendoza, E. MaldonadoBandala, J. Olguín-Coca, L. D. López-Léon, J. P. F. De Los Rios, and F. Almeraya-Calderón, *Metals*, 11 (2021) 105.
29. J. Rodriguez, M. Mouanga, A. Roobroeck, D. Cossement and A. M.G. Olivier. *Corros. Sci.*, 132 (2018) 56-67.
30. X. Liu, J. Sun, Y. Yang, F. Zhou, Z. Pu, L. Li and Y. Zheng. *Mater. Lett.*, 162 (2016) 242-245.
31. Y. Liu Y, H.Y. Li, A.G. *Int. J. Electrochem. Sci.*, 8 (2013) 7753.
32. T. Zandi, H. Verbeken and A. Adriaens. *Int. J. Electrochem. Sci.*, 8 (2013) 548.
33. X. W. Liu, J.K. Sun, K.J. Qiu, Y.H. Yang, Z.J. Pu, L. Li and Y.F. Zheng. *J. Alloys Compd.*, 664 (2016) 444.
34. S. Li, B. Gao, G. Tu, L. Hu, S. Sun, G. Zhu and S. Yin. *Constr Build Mater.*, 71 (2014) 124-131.
35. A.M. Ramirez-Arteaga, J.G. Gonzalez-Rodriguez, B. Campillo, C. Gaona-Tiburcio, G. DominguezPatiño, L. Leduc Lezama, J.G. Chacon-Nava, M. A. Neri-Flores and A. Martinez-Villafañe. *Int. J. Electrochem. Sci.*, 5 (2010) 1786–1798.
36. Ares, A. E. and Gassa, L. M. *Corros. Sci.*, 59 (2012) 290-306.
37. J. Cabral-Miramontes, D.M. Bastidas, M.A. Baltazar, P. Zambrano-Robledo, J.M. Bastidas, F. Almeraya-Calderón and C. Gaona-Tiburcio. *Int. J. Electrochem. Sci.*,, 14 (2019) 4226–4239
38. D. Klotz. *Electrochem commun.*, 98 (2019) 58-62.
39. D.M Bastidas. *Corrosion*., 63 (2007) 515–521.
40. J.R. Scully, D.C. Silverman, M.W. Kendig. Electrochemical Impedance: Analysis and Interpretation STP 1188; ASTM International: Philadelphia, PA, USA, 1993.
41. E.F. Diaz, J.G. Gonzalez-Rodriguez, A. Martinez-Villafañe and C. Gaona -Tiburcio. *J Appl Electrochem.*, 40 (2010) 1633–1640.
42. D.D. Macdonald and S.I. Smedley. *Electrochim. Acta*, 35 *(*1990) 1949–1956.
43. W.R. Osório, C.M. Freire, A. Garcia. *J. Alloys Compd.*, 397 (2005) 179-191.
44. H. Li, X. Xie, Y. Zheng, Y. Cong, F. Zhou, K. Qiu, X. Wang, S. Chen, L. Huang and L. Tian. *Sci. Rep.*, 5 (2015) 10719.
45. E. E. Maldonado-Bandala, V. Jiménez- Quero, F. J. Olguin-Coca, L. G. Lizarraga M, M. A.Baltazar-Zamora, A.Ortiz-C., F. Almeraya C., P. Zambrano R and C. Gaona-Tiburcio. *Int. J. Electrochem. Sci.*, 6 (2011) 4915 – 4926.
46. G. Santiago-Hurtado, M.A. Baltazar-Zamora, R. Galván-Martínez, L. D. López L, F. Zapata G, P. Zambrano, C. Gaona-Tiburcio, F. Almeraya-Calderón. *Int. J. Electrochem. Sci.*, 11 (2016) 4850 – 4864.
47. G.L. Song. *Corros. Sci.*, 52 (2010) 455-480.
48. H. Feng, S. Liu, Y. Du, T. Lei, R. Zeng, T. Yuan, T. *J. Alloys Compd.*, 695 (2017) 2330-2338.
49. A. Martínez-Villafañe, F. Almeraya-Calderón, C. Gaona-Tiburcio, J.G. Gonzalez-Rodriguez and J. Porcayo-Calderón. *J. Mater. Eng. Perform.*, 7 (1998)108-113.
50. M.J. Pellegrini-Cervantes, F. Almeraya-Calderon, A, Borunda-Terrazas, R.M. Bautista-Margulis, J.G. Chacón-Nava, G, Fajardo-San-Miguel, J.L. Almaral-Sanchez, C. Barrios-Durstewitz, A. MartinezVillafañe. *Int. J. Electrochem. Sci.*, 8 (2013) 10697–10710.